Proof-of-Concept In-Situ Diagnostic for Magnetically Shielded Hall Thruster Erosion

Isabella Rieco

A thesis
submitted in partial fulfillment of the
requirements for the degree of

Master of Science

University of Washington

2023

Committee:

Justin Little

Uri Shumlak

Program Authorized to Offer Degree:
Aeronautics & Astronautics

University of Washington

Abstract

Proof-of-Concept In-Situ Diagnostic for Magnetically Shielded Hall Thruster Erosion

Isabella Rieco

Chair of the Supervisory Committee:
Justin Little
Department of Aeronautics & Astronautics

Validating flight-ready hardware for magnetically shielded Hall thrusters is critically dependent on lifetime testing. Traditionally, measuring the erosion of the inner pole requires breaking vacuum, a process that can influence test results, and typically allow for erosion measurements only after extensive durations. A proof-of-concept in-situ erosion diagnostic is explored to assess its feasibility for more accelerated testing. The diagnostic operates by using a conductive material, specifically ITO-coated glass, and tracking the change in its electrical resistance over time. This change in resistance is directly correlated to the material's erosion rate. Testing was conducted under three different operating conditions: 200V, 250V, and 300V in the plume of a magnetically shielded Hall thruster along it's centerline. Theoretical results were also shown for the probe's behavior at the inner pole. The results demonstrated that the resistance change exhibited an inverse trend, in line with theoretical expectations, and the probe was capable of detecting resistance changes as low as 0.05 $\frac{\Omega}{s}$ in the plume and theoretical resolution of 0.04 $\frac{\Omega}{s}$ at the inner pole. Looking ahead, future improvements will focus on mitigating thermal variations and employing more robust materials that erode more slowly, enhancing the diagnostic's durability and accuracy at the inner pole. The successful implementation of this approach — placing a conductor in plasma and measuring its resistance as it erodes — paves the way for the development of in-situ erosion sensors for accelerated Hall thruster lifetime testing.

TABLE OF CONTENTS

LIST OF FIGURES

ACKNOWLEDGMENTS

Thank you to everyone who helped keep me sane with a special thanks to Carlos, Shuba, Bennett, and the IFH community. Thank you Justin for believing in my abilities until the end and to being a great Sherpa. Thank you to the SPACE lab crew for answering my never ending questions and especially to Peter for all the testing help! Special thanks to my other half, Vicente, for your endless support and love.

DEDICATION

to my younger self and for the future...

Chapter 1
INTRODUCTION

Hall thrusters have proven themselves to be a reliable in-space propulsion method. They are already being used on modern satellites and for planetary science missions. This technology, along with the field of electric propulsion, still has many unknown questions about how the plasma behavior affects thruster performance and durability. One of the main concerns with Hall thrusters is their lifetime since this will determine how much total delta-v can be imparted to a spacecraft. The lifetime limiting factor of early Hall thrusters was erosion of the channel walls, which typically begins to limit thruster operation after 4000 hours [13]. Modern Hall thrusters have solved the issue of channel erosion using a technique called magnetic shielding. This refers to a new magnetic topology where the field lines run parallel to the outer channel surfaces and protects them from bombarding species. This invention was able to bring wall erosion rates down significantly to the point where they become negligible compared to the lifespan of the thruster. However, a new type of erosion was observed that is unique to the magnetically shielded Hall thruster, specifically erosion of the inner pole region. Now erosion is once again a main lifetime limiting factor for thruster operation and something to consider while doing lifetime testing. Lifetime testing is something that is vital for validating thruster components and ensuring that the thruster configuration and materials are able to operate during the whole mission duration. Currently, Hall thrusters, along with other electric propulsion thrusters, undergo tens of thousands of hours of full operating time inside a vacuum chamber facility to replicate what it will undergo during a whole mission lifetime. Various measurements are taken while the thruster is on, like thrust or plume characteristics, to understand how the plasma is behaving. To test for erosion of the inner pole, a diagnostic called profilometry is used to create a topographical map of the

surface down to a micro-scale resolution allowing for a very accurate timescale of erosion. However, in order to perform this measurement, testing needs to be halted so that vacuum can be broken and the thruster removed. Needing to stop operation of the thruster could add irregularities to the test along with adding extra uncertainty towards what the plasma's continuous behavior is. Another method that can be used for estimating erosion rates is quartz crystal microbalance. Crystal microbalance works by placing a quartz in the same plane as the inner pole so that it can be bombarded with sputtered particles. The deposited particles then create a change in the resonance frequency of the quartz which allows you to calculate how much mass was deposited. This method can also provide a high level of accuracy for the amount of inner pole that had been eroded off. However, it still requires vacuum to be broken and thruster operation interrupted. Although operation needs to be interrupted, these two methods are still the primary ways to characterize inner pole erosion for lifetime testing of Hall thrusters over the extensive hours it takes for a complete profile.

To address this restraint, the creation of an in-situ erosion diagnostic represents a significant advancement in lifetime testing methodologies, as it negates the need for vacuum breach to gauge erosion levels. Furthermore, this diagnostic's ability to estimate erosion rates more swiftly than traditional techniques substantially benefits the acceleration of lifetime testing processes. Such acceleration is vital for the rapid qualification of thrusters for flight and the streamlining of mission schedules. This thesis describes the development of an in-situ erosion diagnostic that determines erosion rates by monitoring variations in electrical resistance, utilizing a conductive Indium-Tin-Oxide (ITO) coated glass within a modified Wheatstone Bridge circuit. To validate this diagnostic's effectiveness, it was tested within a thruster plume along the inner pole's centerline, and the findings were benchmarked against predictions from a 0D erosion model.

1.1 Magnetically Shielded Hall Thrusters

A Hall thruster is a type of electromagnetic propulsion system that generates thrust by accelerating ions using the Lorentz force. These thrusters typically operate within a power

range of 0.5 to 10 kilowatts and can achieve specific impulse (Isp) values around 2500 seconds. Xenon has traditionally been the propellant of choice due to its inert properties and high atomic mass, which is advantageous for ionization and momentum transfer. However, recent trends have seen a shift towards using Krypton as a propellant due to various factors including cost and availability [19].

The primary components of a Hall thruster include the anode, cathode, and magnetic circuit. The magnetic circuit, which forms a crucial part of the electrical circuit necessary for the thruster's operation, consists of inner and outer annular rings. These create a magnetic field perpendicular to the thruster channel. The anode serves a dual function: it acts as the positive electrode and distributes the neutral propellant into the thruster's channel. It is typically designed with internal channels and symmetric exit holes to allow for the even distribution and ejection of gas into the main channel. The cathode's role is twofold: it acts as an electron source for neutralizing the positively charged plasma that exits the thruster and assists in igniting the propellant. It includes a heater to facilitate thermionic emission, initiating plasma creation within the cathode. Once the plasma is ignited, the heater and keeper are no longer necessary.

Electrons emitted from the cathode have two pathways: some go on to neutralize the high-energy ions being expelled to prevent them from being drawn back into the thruster by the electric field, while others are drawn towards the anode. Those attracted to the anode become trapped by the magnetic field, spiraling along the field lines, which increases their energy. These high-energy electrons then collide with the propellant gas, aiding further ionization and contributing to plasma density. As these electrons move azimuthally, they induce a Hall current. This current interacts with the magnetic field to produce a jxB force along the axis of the thruster, which propels the ions outwards, generating thrust. Figure 1.1 illustrates a cross-section of a Hall thruster, highlighting these components and the process of thrust generation.

Here the cathode is mounted external to the thruster but recent designs have the cathode center mounted creating the region called the inner pole. Additional features not shown

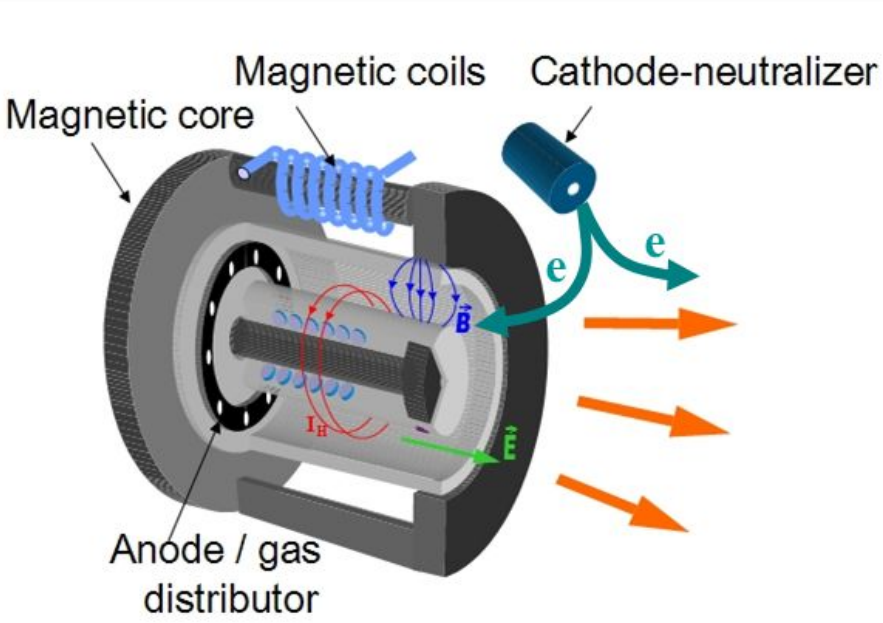

Figure 1.1: Cross section of a Hall effect thruster with an externally mounted cathode. The red lines leaving the thruster denote direction of bulk plasma.

are the insulating layer around the channel walls and external surfaces of the thruster to shield the magnetic circuit. The insulating layer is typically made of either boron nitride or graphite.

1.2 Inner Pole Erosion

Experimental research on magnetically shielded Hall thrusters has indicated that the dominant erosion happens on the center magnetic pole cover. This erosion will affect the magnetic circuit overtime and eventually make the thruster behave erratically, rendering it inoperable for missions [13] [2]. Pole erosion rates are relatively low for high discharge voltages but remain quite high for low voltages [2]. At lower voltages, the acceleration region gets pushed downstream, increasing the production of highly energetic particles in the vicinity of the pole. Laser induced fluorescence (LIF) measurements have shown that ion energies in the near inner pole region are higher than would be predicted from plasma fluid models [1]. It

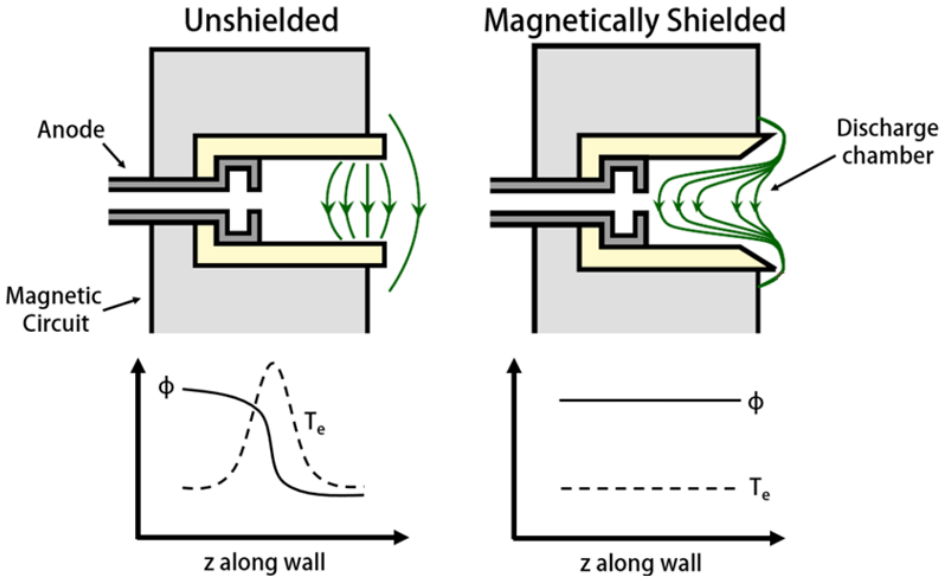

Figure 1.2: Direct comparison of magnetic field configuration of unshielded vs shielded. Electron temperature and plasma profiles along the channel wall for each case are also presented. [6]

is suspected that ions are being heated by instabilities in the channel region which are being directed towards the inner pole across the plasma potential lines [9]. Work by Lopez Ortega et al. using Hall2De, a plasma fluid model, supports this hypothesis [12]. Figure 2 shows the comparison of magnetic field lines between and unshielded and shielded Hall thruster. The shielded version now have field lines that help direct the high energy ion population directly on the inner pole. Whereas, in the unshielded case, you can see the field lines directed the high energy population along the inner channel walls.

Plasma instabilities arise when a source of free energy causes a plasma wave to grow without bound. A study was done by Mikellides et al. that numerically speculates lower hybrid instabilities are the main source of ion heating in the near channel region [16]. The source of free energy was taken to be the relative drift between beam ions and electrons perpendicular to the applied magnetic field [12]. However, the location at which this drift becomes a maximum depends on the plasma structure near the channel exit. Notably, it

has been observed using time-resolved LIF that the ion acceleration region oscillates in and out of the channel at frequencies that correspond to the breathing mode (∼10's of kHz). These oscillations likely have a significant impact on the erosion processes of the center pole since they will influence the rate of particle transport to the pole region in addition to the instability growth rate. Both processes will govern turbulent ion heating and the flux of energetic ions to the pole cover. Recent work by Jorns et al. supports the hypothesis that low-frequency oscillations have a strong influence over turbulence in Hall thruster plasma [7].

1.3 Thesis Scope & Outline

This thesis will begin by detailing the probe design and the rationale for selecting specific materials. Following this, it will present an ideal case scenario using the 0D erosion model, which is predicated on the assumption of constant erosion rates for Indium Tin Oxide (ITO). To enhance the accuracy of the ideal case, measured numbers, such as ion energy distribution, will be used to further validate the model. Subsequently, the prototype and its experimental setup for data collection will be introduced along with results. After the experimental procedures, the thesis will delve into a discussion of the numerical results, comparing them to both the ideal case and existing lifetime testing outcomes. The final sections will explore potential design improvements, future research directions, and alternative applications. The development and refinement of lifetime testing for Hall thrusters are crucial steps towards expediting mission schedules and confirming the readiness of hardware for spaceflight.

Chapter 2
ITO PROBE CONCEPTS

Pole erosion is difficult to characterize because it happens over very long-time scales. Typical erosion rate measurements are made by running the thruster at a set operating point for durations in excess of 500 hours. Tests are then interrupted to perform ex-situ measurements of the surface geometry using a high sensitivity profilometer. This conventional approach is clearly not conducive to rapid testing across a variety of operating points [4]. To address this problem, we will develop a new sensor that is capable of detecting erosion rates in-situ on timescales less than 15 minutes. The sensor will use indium-tin-oxide (ITO) coated on glass, ideally mounted such that its surface is flush with the center pole, tested in the plume along thruster centerline. Since the resistance of this circuit is inversely dependent on the cross-sectional area of the coating, as the ITO erodes, we will be able to use a bridge circuit to measure the increased resistance versus time, yielding the erosion rate.

2.1 Indium Tin Oxide

Indium-Tin-Oxide (ITO) coated glass, renowned for its electrical conductivity and optical transparency, is a prime material for thermally sensitive electronic applications. ITO, a mixed oxide of indium and tin, typically exhibits a melting point ranging from 1526–1926 °C, depending on its composition. It's an n-type semiconductor with a large bandgap of around 4 eV, making it transparent to visible light while retaining significant conductivity [14]. ITO's low electrical resistivity, approximately $10^{-4}\ \Omega cm$, coupled with its ability to maintain over 80% optical transmittance in thin film form, makes it advantageous for touch-screen applications such as in mobile phones. Low electrical resistivity also makes the material very sensitive to any resistance change allowing high resolution measurements more attainable.

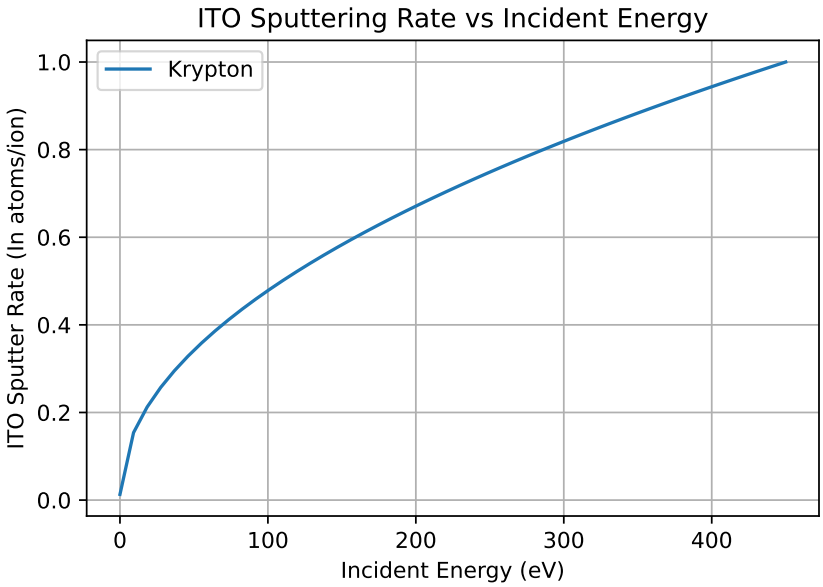

Figure 2.1: Sputtering rate of ITO for incident Krypton ions based on the model from [10].

The coating of ITO on glass substrates is predominantly achieved through physical vapor deposition techniques. Sputter deposition, one of the most commonly used methods, allows for the creation of thin films with controlled thickness, essential for maintaining a balance between conductivity and transparency. This balance is crucial since increasing the film's thickness or the concentration of charge carriers enhances conductivity but reduces transparency. Since ITO has a high electrical conductivity, it is very sensitive to any change in coating thickness due to erosion. A study was done to examine ITO sputtering rates from different ion sources at different incident energies. Figure 2.1 shows the main result of their work for common noble gases. A model was used based on an arbitrary atomic mass to model the sputtering rate over different incident energies. The sputtering rate has units of Y$[\frac{atoms}{ions}]$ and E, the incident energy, is in [eV]. The equation used to fit the data is:

$$Y = A(m)(E^{\frac{1}{2}} + E_{th}^{\frac{1}{2}}(m)) \tag{2.1}$$

Where E is the ion incident energy, A is a proportional constant, and E_{th} represents the threshold energy. The parameters A and E_{th} depend on a general atomic mass of the incident ions, m. $E_{th}^{\frac{1}{2}}(m)$ and $A(m)$ are defined by:

$$E_{th}^{\frac{1}{2}}(m) = am^b \tag{2.2}$$

$$A(m) = am^2 + bm \tag{2.3}$$

Where a=36.68 and b=-1 for $E_{th}^{\frac{1}{2}}(m)$ and $a = -1.39 \cdot 10^{-5}$ and $b = 1.25 \cdot 10^{-3}$ for $A(m)$ [10]. Applying this model to Krypton will show how the ITO glass will be sputtering during this experiment. The sputtering rate is shown in Figure 2.1 and is used in the 0D erosion model described later on in this Chapter.

2.2 Circuit Design

The Wheatstone Bridge is an electrical circuit used to precisely measure, on a resolution of $> 10m\Omega$, an unknown electrical resistance by balancing two legs of a bridge circuit [8]. The traditional Wheatstone Bridge has a diamond-shaped configuration with four resistors: one unknown, two known, and one variable. The bridge leverages a galvanometer to detect zero current flowing through the bridge, at which point the unknown resistance can be calculated using the known and variable resistances. When the circuit is balanced, the relationship between resistors is:

$$\frac{R_1}{R_2} = \frac{R_3}{R_4} \tag{2.4}$$

where R_3 and R_1 are the known resistors, R_2 is the variable resistor, and R_4 is the unknown resistor. However, the design can be adapted for different applications. In a modified version of the Wheatstone Bridge, instead of a variable resistor and a galvanometer, three known resistors are used along with a voltage measurement between two points.

This modification still allows for the calculation of an unknown resistance but uses voltage difference (ΔV) in the calculation. Solving circuit equations gives a relationship between the ΔV, the 3 known resistors, and the unknown resistor:

$$\Delta V = V_s \left(\frac{R_3}{R_3 + R_4} - \frac{R_2}{R_1 + R_2} \right) \tag{2.5}$$

where V_s is the applied voltage, R_1, R_2, R_3 are the known resistors, and R_4 is the unknown resistor (or the probe). We can rearrange this equation to solve for the unknown resistance:

$$R_4 = \frac{R_2 \cdot V_s - (R_1 + R_2)\Delta V}{R_1 \cdot V_s + (R_1 + R_2)\Delta V} \cdot R_3 \tag{2.6}$$

When implementing this design, factors such as wire resistance and temperature come into play, potentially affecting the accuracy of the resistance measurement. To mitigate these issues, a three-lead design can be employed. Figure 2.2 shows the electrical circuit used along with the 3-lead design. In this design, two of the leads are connected in series with each leg of the bridge, ensuring that if these leads are of equal length and temperature, their resistances will be equal, thus maintaining the balance of the bridge. The third lead is used solely for voltage sensing and does not influence the stability of the circuit.

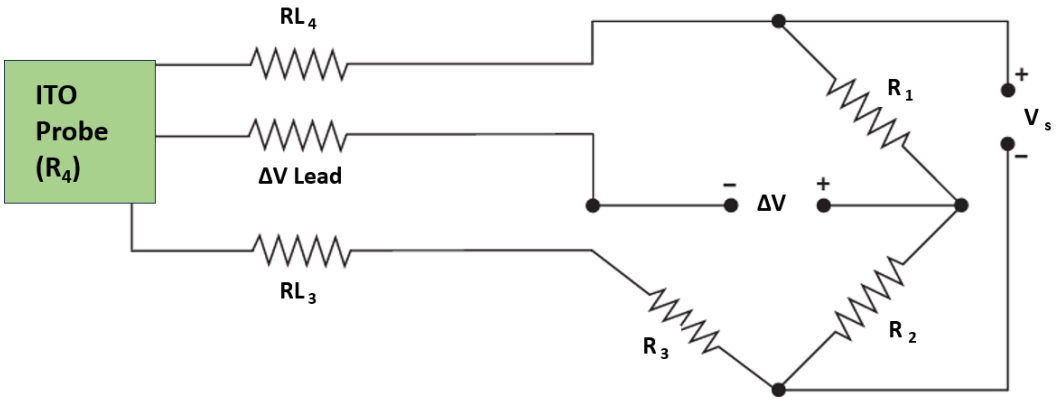

Figure 2.2: Schematic of the circuit used during experimentation.

This three-lead approach offers a balanced bridge that is not affected by thermal or

resistance changes in the long wires, allowing for high-resolution measurements of an unknown resistance without the need for a variable resistor [17]. This is particularly useful for probing applications where the probe acts as the unknown resistor and is connected to the circuit via feedthrough leads that are very long, like in my case.

2.3 0D Erosion Model

A data-informed model is necessary for understanding plasma behavior in relation to the system. This model will also give predictive results for how well the ITO probe can resolve erosion rates and resistance changes at the inner pole. Like any model, the results highly depend on the initial conditions and validation from experimental results to improve the accuracy of plasma behavior predictions. The initial conditions for this model depend on the ion current density, ion energy distribution, and physical sizing of the ITO glass. We can see these dependencies get reflected through the following equations used to describe the resistance change and erosion behavior.

Starting with understanding how to find resistance and how this value will change with time and exposure to the plasma. Resistance is defined as:

$$R_0 = \frac{\rho \cdot L}{A} \tag{2.7}$$

where ρ is the resistivity and an inherent property of the material. L is the length where that resistance is being held and A is the effective area. In this case, L is the length of the glass substrate and A is the effective area that current is being applied to. Figure 2.3 shows the dimensions in action and where they are on the ITO glass. The cross-sectional area, A, is the product of the width with the change of thickness over time. The resistance changes as the thickness erodes changing the respective area. Knowing that the thickness will change as erosion occurs we can denote this with:

$$T(t) = T_0 + \epsilon \cdot t \tag{2.8}$$

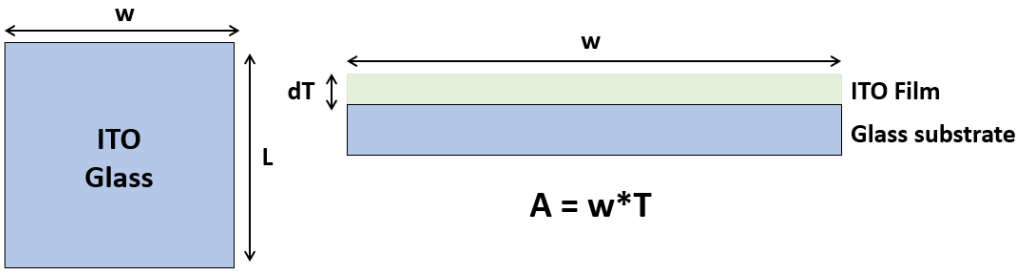

Figure 2.3: Top (left) and side (right) view of the ITO glass substrate.

where T(t) is the thickness with respect to time and T_0 is the initial thickness. Subbing this into the resistance equation and rearranging gives a relation for how resistance changes as the thickness erodes:

$$R(t) = R_0 \left(\frac{T_0}{T_0 - \epsilon \cdot t} \right) \tag{2.9}$$

where T_0 is the initial thickness of the coating, ϵ is the erosion rate and t is time. Knowing the relation of resistance change over time will give us predictive results on both how quickly the ITO will erode but also the behavior of erosion as time goes on. The erosion rate is defined as:

$$\epsilon = \frac{j_i \cdot w}{\rho \cdot e \cdot A_v} \cdot Y(E) \tag{2.10}$$

where Y(E) $[\frac{atoms}{ion}]$ is the sputtering rate for ITO from incident krypton ions at a specific energy. This value and relation was discussed in the previous section. W $[\frac{g}{mol}]$ is the atomic weight of ITO, ρ $[\frac{g}{cm^3}]$ is the mass density of ITO, A_v is Avogadro's number, and j_i $[\frac{A}{m^2}]$ is the ion current density for the incident ions interacting with the glass surface area. This will give us an erosion rate on the order of $[\frac{\mathring{A}}{s}]$. For ITO, w = 428 $[\frac{g}{mol}]$ and ρ = 6.8 $[\frac{g}{cm^3}]$.

2.3.1 Inner Pole Estimations

Since the aim of this thesis is to provide a proof-of-concept, the experiment, outlined in Chapter 3, was conducted in the far plume to test how the probe would output while interacting with plasma. The ultimate goal, however, is to position the probe on the inner pole of a magnetically shielded Hall thruster to directly measure resistance changes, as this location is subject to erosion.

To evaluate the probe's performance at the inner pole, we can apply the 0D erosion model to see how the probe will behave while at the inner pole of a magnetically shielded Hall thruster. Predicting what the sensor would do at the inner pole will help explore the viability of the design. Data used in the model was taken from a study done on the magnetically shielded miniature Hall thruster (MaSMi) where they obtained the ion energy population and ion current density at the inner pole using laser induced fluorescence (LIF) [11]. LIF is a diagnostic tool that works by collecting the fluoresced ions excited from an incoming laser. The paper measured the ion current density and ion energy distribution at the inner

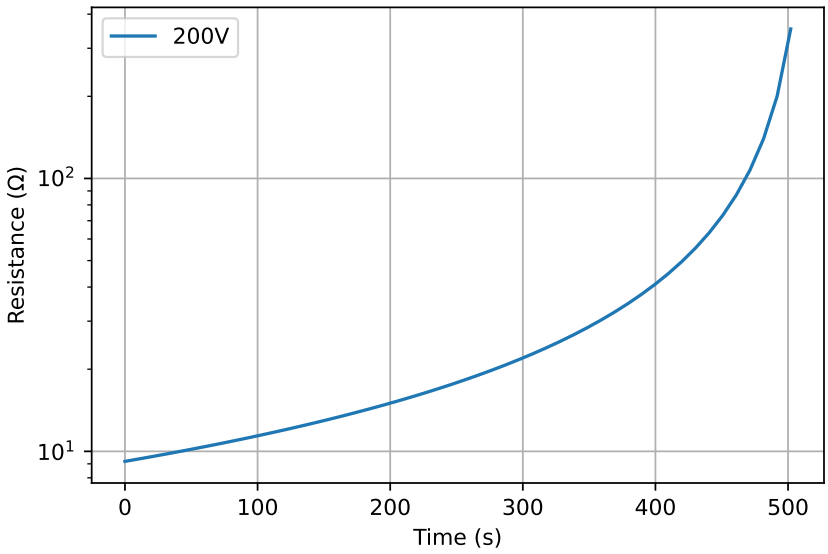

Figure 2.4: Estimated resistance vs time at the inner pole.

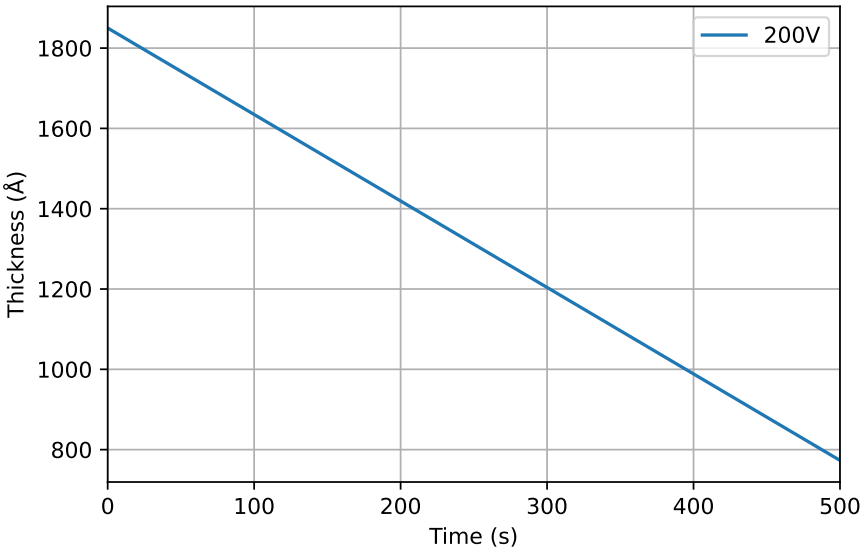

Figure 2.5: Estimated thickness vs time at the inner pole.

pole for MaSMi operating at 200V and 1A, so similar to the conditions that the 200V case underwent shown in Chapter 3. They reported an ion current density of 0.8 $\frac{A}{m^2}$ and an average ion energy of 210eV at the inner most point on the inner pole. Incorporating these findings into our model for the ITO concept probe, we observed a resistance-over-time trend (Figure 2.4), assuming Xenon propellant usage, as in the MaSMi study [11]. The model reveals that the sensor can detect resistance changes within the first 50 seconds, with an estimated lifespan of about 500 seconds at the inner pole and a resolution of 0.04 $\frac{\Omega}{s}$. This resolution is found by taking the difference between the smallest resistance change observed and dividing it by the time it took to detect that change. Additionally, Figure 2.5 illustrates the expected thickness variation of the sensor at the inner pole.

It's important to compare the erosion rate of ITO, as predicted by our model, with the observed erosion rate of the graphite inner pole in the MaSMi study. A long duration wear test was conducted under operating conditions of 200V and 1A for a total of 400 hours [5]. The average erosion rate at the innermost point of the graphite inner pole, measured using

optical profilometry, was found to be 205 $\frac{\mu m}{khr}$ which corresponds to .57 $\frac{\mathring{A}}{s}$. In contrast, our model predicts an erosion rate of 3.6 $\frac{\mathring{A}}{s}$ for ITO at the inner pole. Despite the order of magnitude difference between these two rates, they can still be meaningfully compared by scaling them relative to each other. This comparison is crucial for evaluating the suitability of ITO as a material for estimating inner pole erosion in similar applications.

Chapter 3
THE PROTOTYPE

This thesis presents a proof-of-concept for an in-situ erosion diagnostic tool designed to measure erosion rates through changes in electrical resistance. The probe operates on the principle that as a conductor erodes, its resistance alters, providing a quantifiable measure of erosion rate. To explore the interaction between the conductor and plasma and validate if resistance changes correlate with erosion rates, the probe was positioned in the far plume of the thruster. Although the ideal placement for such a probe would be around the inner pole, where thruster erosion predominantly occurs, this setup provides a suitable testing environment.

This chapter first details the design of the probe and the materials selected for its construction, emphasizing their relevance to the intended application. Following this, it elaborates on the experimental setup and the procedures followed during testing. This includes descriptions of both the specific thruster model utilized and the vacuum facility where the experiments were conducted.

3.1 Probe Construction

The design of the probe is centered around minimizing plasma disturbance and preventing current draw from the plasma during thruster operation. It comprises of three key components: a Teflon cover, ITO coated glass plate, and a water cooling block.

The front-facing Teflon cover shields most of the probe from direct plasma contact. Teflon was chosen for its insulating properties and structural strength. This cover features a central window, exposing the ITO glass, which is the primary site for erosion. The ITO glass, a 25x25 mm square with a conductive coating on one side, is snugly positioned between the

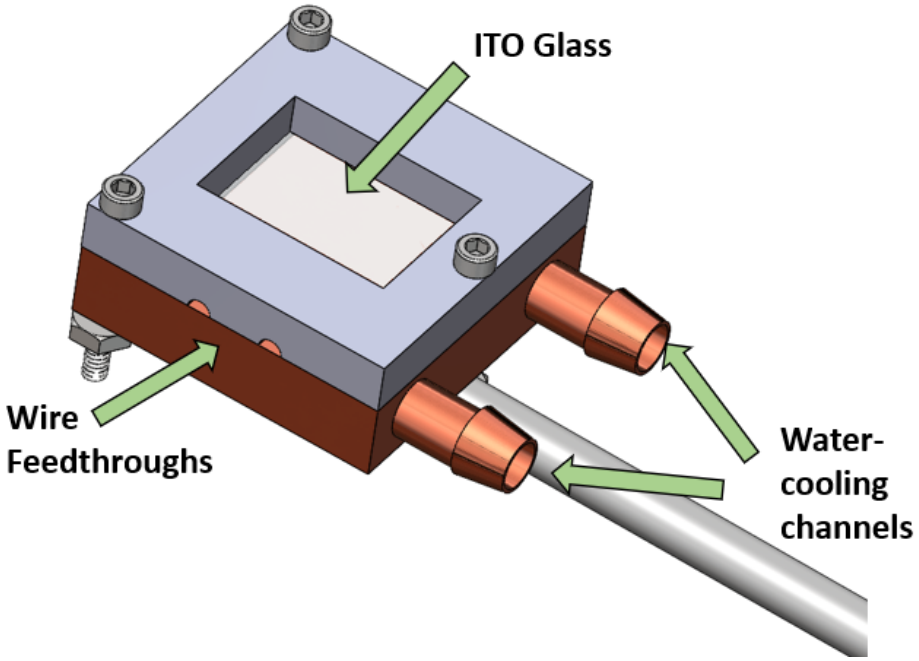

Figure 3.1: SOLIDWORKS model of the ITO sensor prototype.

Teflon cover and the water cooling block beneath. A small lip in the Teflon cover, extending about 10 mm on each side, creates a compression fitting for the glass.

To integrate the ITO glass into the circuit, wires are soldered onto copper tape that is tightly pressed against the glass, ensuring both solid electrical and thermal connections. This compression also secures the glass to the water cooling block, facilitating consistent temperature maintenance.

Figure 3.1 shows the final design of the erosion sensor. The assembly of the probe includes securing it to a solid stainless steel rod using both a through-hole and a U-clamp. The Teflon, along with the copper block and stainless steel rod, are held together firmly by three bolts that run through all these components. The bolts are 4-40 1 inch long Nylon screws that are rated up to 180 °C. Nylon was chosen so that the screw, similar to the Teflon cover, would be insulated from the plasma to not give additional current paths. Lastly, the wires from the copper tape extend along the probe arm and are secured against the arm with

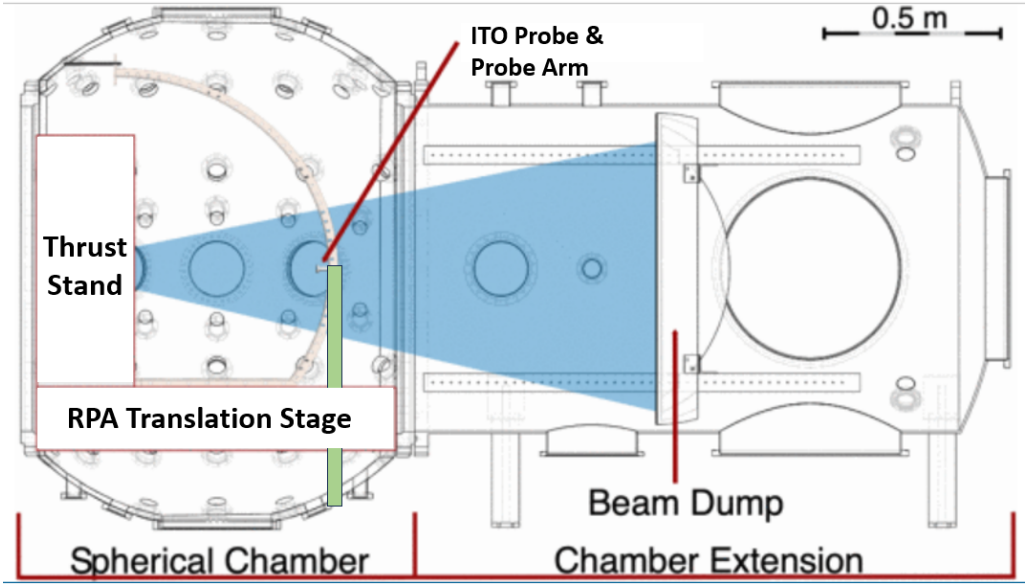

Figure 3.2: Schematic of the experimental layout from a top-down view. The green box denotes the probe arm.

zipties so they are stable during arm rotations. All plasma facing surfaces along the arm are coated in graphite for shielding against plasma interactions, ensuring stable and accurate measurements.

3.2 Experimental Setup

Figure 3.2 is a schematic of the experimental layout inside the Space Test Facility (STF). The thrust stand is where the Hall thruster is placed, the blue is the plume, and the green bar is where the probe arm is. The probe arm is affixed to a rotational vacuum feedthrough, enabling the probe's face to rotate in and out of the plasma for experimentation. This mechanism is illustrated in Figures 3.3 and 3.4, which depict the probe's different operational orientations. Additionally, a retarding probe analyzer (RPA) is employed to ascertain the ion energy distribution at the point where the plasma interacts with the ITO glass. The RPA functions through a series of filters and collection grids. Ions with varying energies impact the aperture at different depths, generating distinct signals that are measurable [20].

When the ITO sensor is retracted to its resting position, the RPA, mounted on a translation stage, can be positioned in front of it, aligning with the same plane.

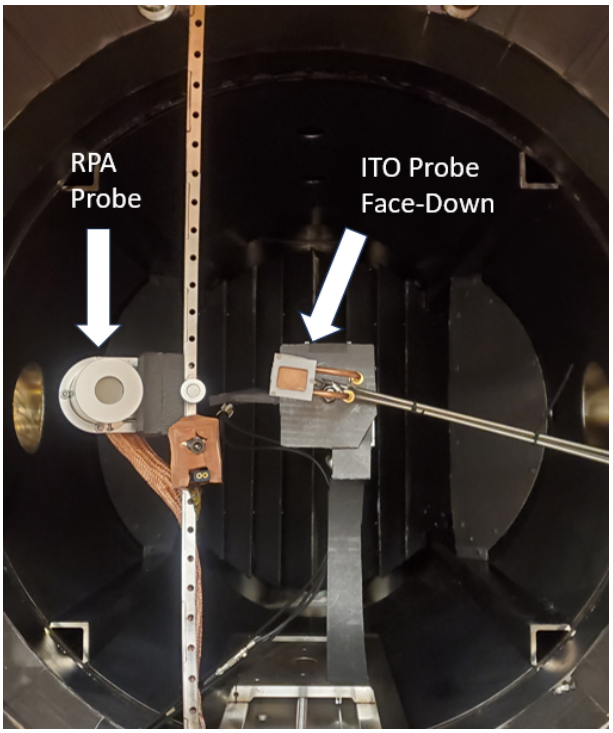

Figure 3.3: ITO prototype while rotated towards the plume in-line with thruster centerline.

The internal setup of the chamber is shown in Figures 3.3 and 3.4. Figure 3.3 captures the probe oriented towards the plasma plume, aligning it with the thruster's centerline. Visible in the same image is the RPA attached to the translation stage. Figure 3.4, conversely, displays the probe faced upwards, away from the plume. Additionally, graphite tape is applied along the arm to safeguard all wiring and the plastic water line tubes from plasma interactions.

The testing process begins with the probe in an upward, relaxed position. It is then rotated inward to face the plasma plume directly. Various tests were conducted with the probe exposed to the plasma for durations of 10, 30, and 60 seconds. Throughout these intervals, an oscilloscope recorded differential voltage measurements. These tests were repeated across thruster voltages of 200, 250, and 300 volts while current was held constant at 1.66 A.

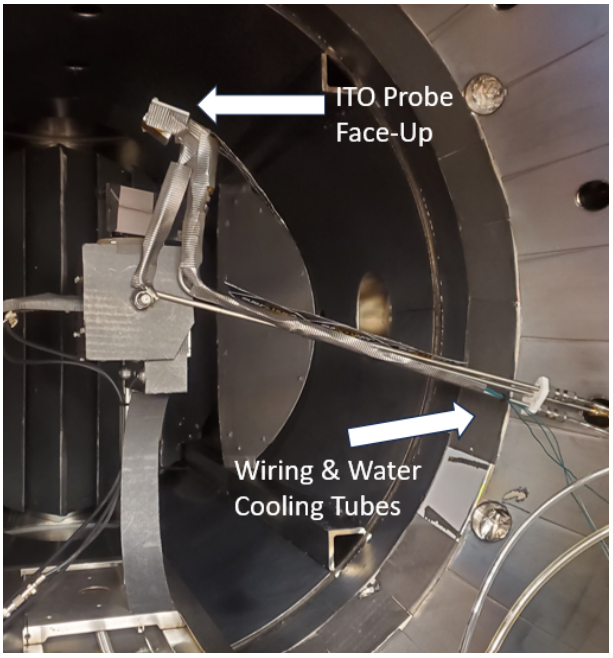

Figure 3.4: ITO prototype while rotated up in resting position clear of the plume.

Voltage measurements were taken before and after each exposure to the plasma. For two of the voltage settings, continuous measurements were captured while the glass was subjected to the plasma. The voltage supplied to the circuit was also consistently monitored via the oscilloscope.

3.2.1 ACME Thruster

The Adaptive-field Central-cathode Magnetically-shielded Electric thruster (ACME), depicted in Figure 3.5, was developed to explore the impact of various magnetic field shapes in Hall thrusters [18]. ACME's unique design allows for the adjustment of its magnetic fields in two ways: by varying the current in the inner and outer electromagnets and by physically altering the position of the inner and outer poles relative to each other. This adjustment is facilitated by a magnetic circuit interface located at the thruster's rear, enabling each pole to move as a single unit. This ensures that, regardless of the poles' positions, the magnetic

shielding profile remains uniform. The currents in the magnetic coils of both the inner and outer poles are carefully balanced to modulate the field's strength and magnitude according to the position of the poles. These positions are designated based on the location of the inner pole relative to the outer, with the 0mm position indicating alignment on the same plane. The design of the magnetic shielding in ACME draws similarities to that of JPL's MaSMi and shielded versions of the H6 thruster [3] [15]. During testing the thruster was kept to the 0mm position over the voltage ranges of 200, 250, and 300 V and 1.66A.

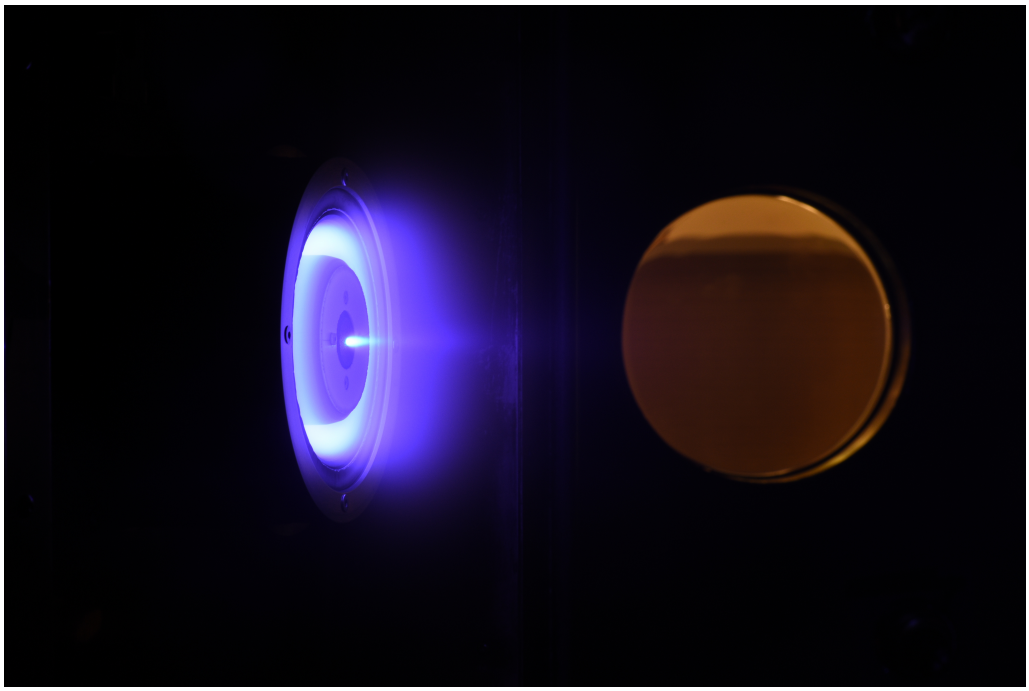

Figure 3.5: ACME thruster in operation at 300V and Krypton propellant.

3.2.2 Vacuum Facility

The evaluation of the thruster was conducted in the SPACE lab's 5 cubic meter Space Test Facility (STF). A schematic of this chamber can be seen in Figure 3.2. This chamber is equipped with a Shimadzu turbopump located at the lower end of its extension and two Sumitomo cryopumps positioned strategically behind the beam dump. This configuration

allows for an impressive total pumping speed of 12,000 liters per second for Krypton. Pressure levels within the chamber are meticulously monitored using a nude ion gauge situated behind the thruster's exit plane. This gauge is effectively protected from the beam plasma by a shroud that surrounds the thrust stand. Additionally, a cold cathode gauge placed just downstream of the exit plane and a Residual Gas Analyzer (RGA) located behind the beam dump provide supplementary pressure readings. During the testing phases, the facility consistently achieved a base pressure of $5 \cdot 10^{-7}$ Torr, a level maintained during each vacuum cycle that occurred between changes in the thruster setup.

3.3 Experimental Results

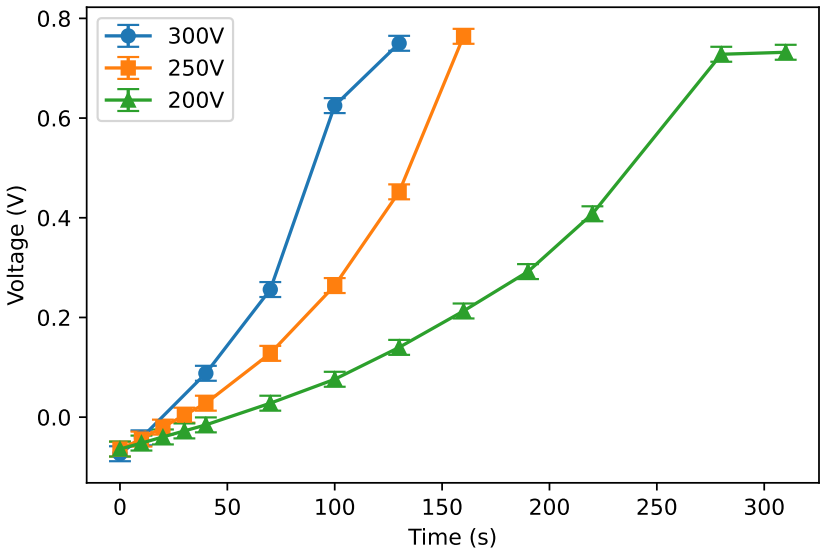

Figure 3.6: Voltage vs time measurements for all three test cases.

Voltage measurements were systematically taken before and after each exposure of the glass to the plasma plume, tracking its performance over its lifespan. These measurements, which are presented in Figure 3.6, reflect the voltage changes under different thruster operating

conditions. For all test cases, the supplied voltage was maintained at a constant $V_s = 1.52V$. The resistors were set at: R_1=R_2 = 101.18 Ω, and R_3 = 10.84 Ω for every test.

The initial voltage measurement was contingent on the starting resistance of the ITO glass, with all three cases beginning around -55 mV. The starting resistance for the ITO coating, as per the manufacturer, was between 7-10 Ω. As the ITO film underwent complete erosion, the voltage escalated to 750 mV. This value, representing half of the input voltage, indicated that one branch of the Wheatstone bridge had effectively become an open circuit. Consequently, the voltage difference measured was only between one arm of the circuit, across equal resistors R_1 and R_2 which is the expected outcome after full erosion occurs. This progression is also mirrored in the plot depicting voltages over the test duration. For the 200V case, the test was continued after reaching 750 mV to confirm this result and to study the probe behavior fully eroded while in the plume. As expected, a constant average voltage was measured during the whole exposure time while the thickness was depleted. The resolution restraints on the oscilloscope provided an error of ± 15 mV.

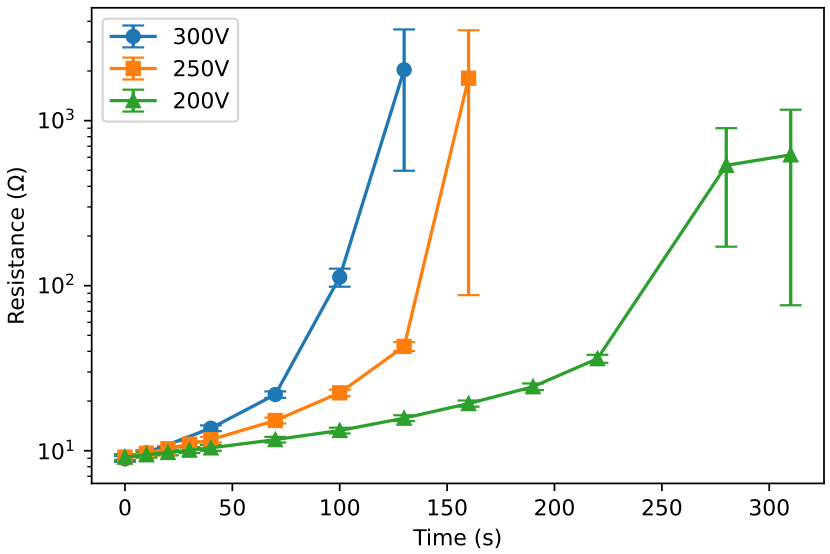

Figure 3.7: Calculated resistance vs time for all three test cases.

Figure 3.7 showcases the corresponding resistance values derived from these voltage measurements. The error bars are dramatically large for the last points since that value is reaching a theoretical infinity which artificially inflates the error for that point. Initially, resistances were observed in the 7-10 Ω range, as anticipated. The smallest resolved change in resistance detected was during the 250V case. A change of 0.5 Ω was measured over a 10 second exposure time giving this probe a resolution of 0.05 $\frac{\Omega}{s}$. As the ITO film experienced further erosion, there was an inversely dependent increase in resistance. This is due to the relationship between resistance and thickness changes. The other factor that can affect this is the erosion rate which is dependent on the ion current density and ITO sputtering rate for that incident energy. The graph illustrates that upon complete erosion of the film, the calculated resistance sharply increases, tending towards the theoretical infinity associated with an open circuit. This data provides insightful trends regarding the erosion process and the electrical behavior of the ITO film under test conditions.

3.3.1 RPA Probe Results

In each test campaign, a Retarding Potential Analyzer (RPA) played a crucial role in determining the incident ion energy distribution and ion current density. This information is vital for understanding the plasma environment the probe is exposed to. The RPA functions by selectively allowing ions of specific energies to pass through, thus enabling the measurement of ion energy distributions. The data captured by the RPA was recorded using an oscilloscope, which provided detailed insights into the voltage versus current characteristics of the ions and is shown in Figures 3.8, 3.9, and 3.10 below. To ensure the accuracy and reliability of the results, the data plot underwent a filtering process. This step was essential to eliminate any high-frequency oscillations that could potentially distort the analysis. After filtering, the data was normalized to facilitate easier interpretation and comparison.

The derivative of this measured signal is a critical component of the analysis, depicted in blue on the plot. This derivative graphically represents the ion energy distribution, offering a clear view of the range and intensity of ion energies present in the plume at the exact

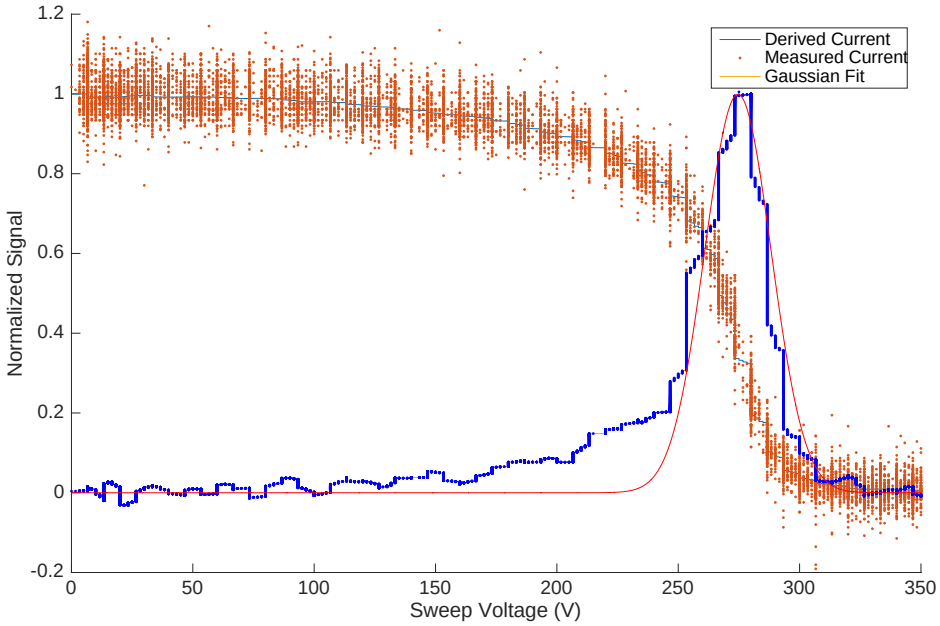

Figure 3.8: RPA results for 300V.

probe location. To further validate the experimental data, a Gaussian fit was applied to this calculated distribution. This fitting process involved overlaying a Gaussian curve onto the experimental data, providing a visual and quantitative comparison to theoretical predictions. The degree of congruence between the Gaussian fit and the experimental data offers valuable insight into how closely the experimental conditions align with theoretical expectations. For each graph the peak energy that the RPA measured is the total energy potential that the initial thruster condition put in.

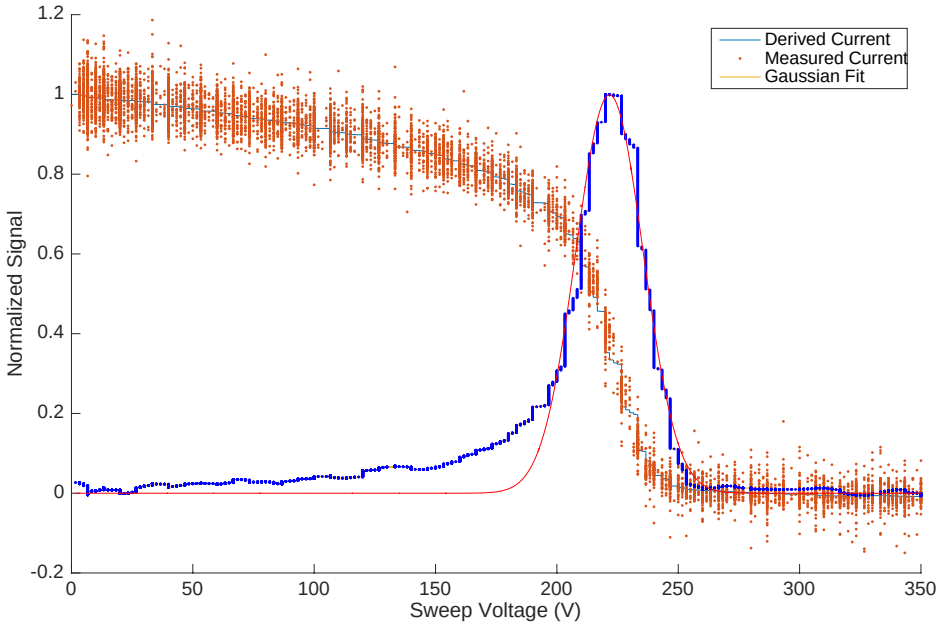

Figure 3.9: RPA results for 250V.

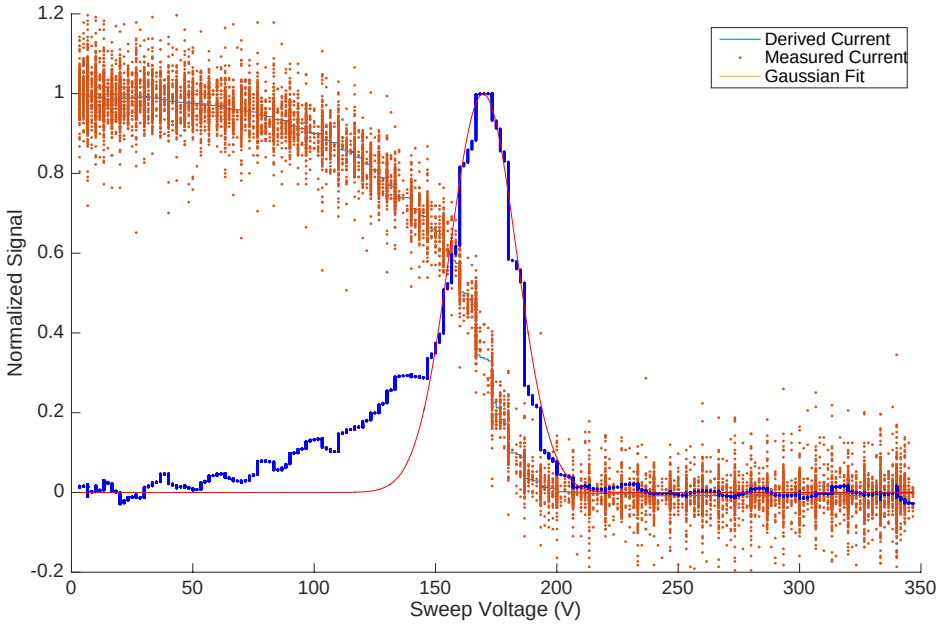

Figure 3.10: RPA results for 200V.

Chapter 4
THE IDEAL CASE

This proof-of-concept experiment demonstrates the feasibility of using an ITO glass substrate to detect erosion within a plasma environment over a period of minutes. However, it prompts the question: how would this system perform under ideal conditions? The core concept of this experiment is to place an eroding conductor in the plasma, then observe changes in resistance as the plasma interacts with the material. In an ideal setup, this conductor would be concentrically positioned around the inner pole cover of a magnetically shielded Hall thruster. Under these conditions, the material would erode at a near-constant rate, allowing for more accurate resistance measurements, as the circuit would maintain a floating potential relative to the plasma. This consistent erosion rate is crucial for the predictive model to effectively represent the material's behavior over time. This chapter will explore the idealized scenario for the ITO film, presuming a uniform erosion rate based on specific ion properties and how this compares to experimental results.

4.1 Numerical Results

In Chapter 2, the 0D erosion model provided a theoretical framework for predicting the erosion behavior of ITO glass under specific plasma conditions. Using this model, we can calculate and predict how the ITO glass erodes. Table 4.1 details the initial conditions and plasma parameters relevant to this analysis while Figure 4.1 shows the resulting resistance over time trend where the lines are theoretical results. Notably, the plot shows a cutoff point corresponding to the complete erosion of the coating, marking a singularity in the model and the end of our predictions.

There are two key observations from these predictions. First, the model's forecasted

	Y $[\frac{atom}{ion}]$	$\epsilon[\frac{\mathring{A}}{s}]$	E_i [eV]
300 eV	0.82 ± 0.05	18.73 ± 0.1	275 ± 0.5
250 eV	0.75 ± 0.05	12.24 ± 0.1	225 ± 0.5
200 eV	0.67 ± 0.05	7.32 ± 0.1	165 ± 0.5

Table 4.1: Values used to find predicted resistance vs time rates.

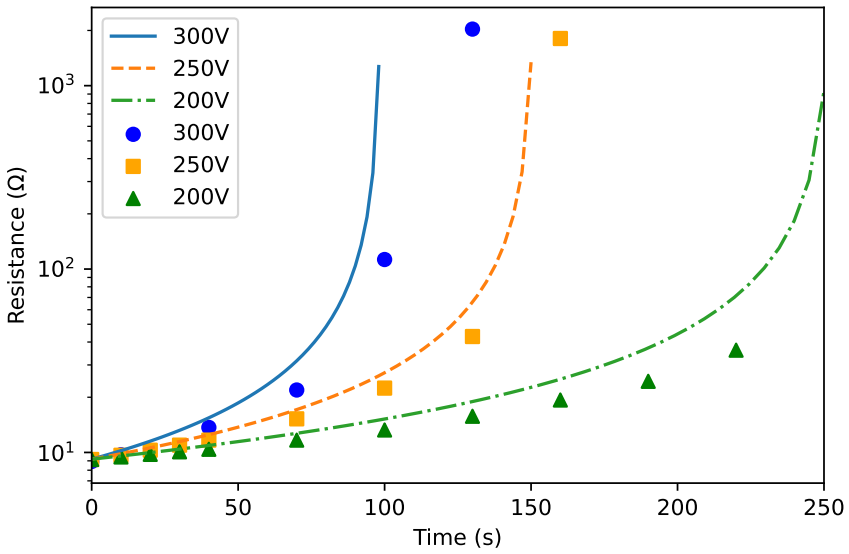

Figure 4.1: Predicted resistance change with experimental data overlayed over time.

probe lifetime aligns with the experimental data, both indicating a total duration of a few minutes. Second, the model predicts an inverse trend in resistance change, which is in agreement with the experimental findings. By overlaying the experimental data on these trends, as shown in Figure 4.1, we can make a closer comparison. This direct comparison reveals two things: the predicted end of the probe's lifetime is shorter than what was experimentally observed, and the estimated resistance change shows a marginally steeper slope compared to the experimental trend. The driving term for the steeper slope in the theoretical results is the calculated sputtering rate for ITO. The sputtering rate used in the

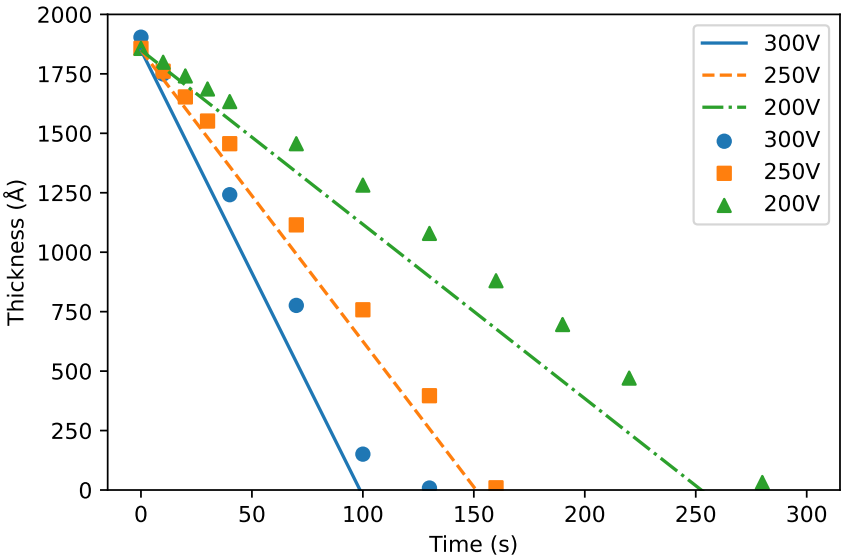

Figure 4.2: Predicted thickness vs time with experimental data overlayed.

model assumed an incidence angle of 0° and that all incident ions had the same energy. Considering that the probe was perpendicular to the plume assuming an incident angle of 0° is a safe assumption. Whereas, majority of error would come from not accounting for the distribution of incident energies while calculating sputtering rate. Figure 4.2 shows the resulting experimental thickness change over time with the predicted thickness change. Similar patterns are observed for the thickness change where the predicted rates are more steep than what's measured. For all three cases, the initial point is 1850 $\mathring{A}$ which is the initial coating of the ITO film.

Despite these discrepancies, the strong correlation between the predictive model and the experimental results validates our ability to accurately model and predict the resistance changes of ITO glass in a plasma environment. The experimental results indicate a longer lifetime than predicted, which can be attributed to the time measurement uncertainties in the experiments. In all three cases, the probe's readings plateaued at 750mV before the campaign's conclusion, suggesting that the predictive model's results might more accurately

reflect the probe's total lifetime. Another aspect to note is the sputtering rate for ITO from krypton propellant was calculated using the average incident ion energy. In realty, there is a whole range of incident energies bombarding the probe each at their own sputtering rate. This variability is another reason the experimental results fall below the predicted rate.

4.2 Discussion

The experimental and theoretical results both support the potential of using an eroding conductor as an erosion sensor within a plasma environment. Experimentally, it has been demonstrated that when the circuit is floating, it can detect resistance changes without drawing significant current, thereby preserving the integrity of the results. Theoretically, the sensor is capable of detecting these resistance changes on a much shorter timescale compared to traditional methods, which typically require hundreds of hours of erosion testing.

An interesting aspect to consider is the behavior of the measured voltage signal when the sensor is exposed to the plasma. Figure 4.3 and 4.4 illustrates this, showing the signal and corresponding resistance change during the 200V test, approximately 60 seconds in. In this test, the probe entered the plasma at 10 seconds and exited at 40 seconds, totaling 30 seconds of exposure. The measured signal reveals two distinct jumps – one occurring while the probe was in the plasma and another occurring after its removal. These jumps are believed to be caused by thermal variations in the probe, despite it being water-cooled. The ITO plate is connected to the circuit via a compression fitting, and even slight thermal changes can significantly alter this compression once a certain thermal threshold is surpassed. These jumps are evident in Figure 4.3, both during and after plasma exposure. The initial jump at t=20 seconds indicates a weakening of the signal due to the fitting's change, leading to a recording of a higher voltage change than what actually occurred. Conversely, after the probe's removal at t=40 seconds, it appears to cool down sufficiently to revert to its original compression state. Post-jump voltage readings are considered more accurate as they reflect the true resistance change.

Additionally, to further investigate the thermal effects on the probe, an infrared (IR)

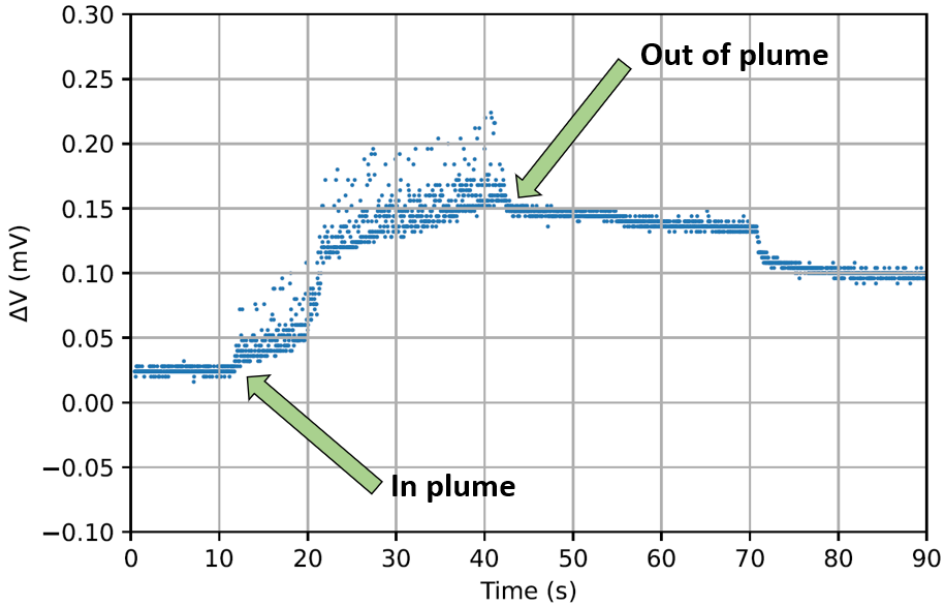

Figure 4.3: Continuous measurement of ΔV vs time while the probe was in the plume.

camera was used to monitor the probe's temperature during the end of the 250V campaign after 140s of total exposure time. The probe remained in the plasma, and its temperature was measured every 10 seconds for a minute. Figure 4.5 presents these findings, indicating a consistent linear increase in temperature with each exposure to the plasma. This evidence bolsters the hypothesis that thermal conditions play a significant role in the sensor's performance and the observed voltage signal changes along with further measures needing to be taken to mitigate thermal changes. The thermal effects would need to be solved before exploring the possibility of discerning erosion rate measurements while exposed to the plasma.

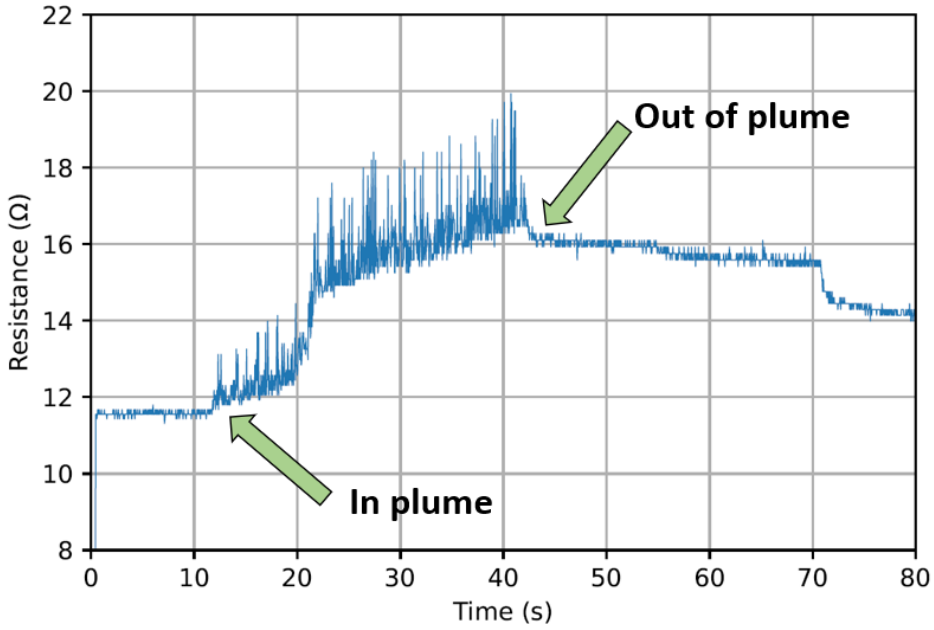

Figure 4.4: Calculated resistance vs time based on Figure 4.4.

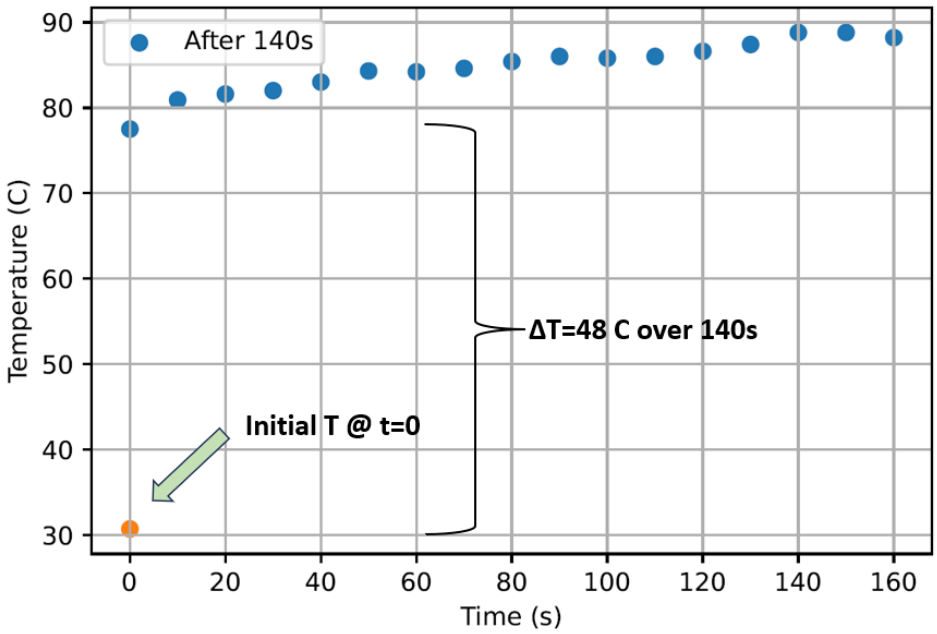

Figure 4.5: Measured temperature after 140s long campaign at 250V.

Chapter 5

CONCLUSION & FUTURE WORK

Hall thrusters are increasingly favored for long-duration spaceflight missions due to their efficiency as electric propulsion systems. A critical step in preparing these thrusters for flight is extensive lifetime testing, which ensures the operational reliability of the flight hardware. A significant factor in this testing is monitoring the erosion rates of the inner pole cover, a process that traditionally requires hundreds of hours and often necessitates interrupting the vacuum conditions, impacting the overall testing accuracy. This thesis introduces a novel diagnostic approach aimed at enhancing the efficiency of lifetime testing for Hall thrusters. The proposed proof-of-concept diagnostic eliminates the need to break vacuum and aims to provide more rapid erosion rate measurements that could significantly accelerate the lifetime testing process.

The diagnostic tool was strategically positioned in the far plume, along the centerline of the thruster, to assess whether a conductor exposed to plasma could effectively measure and discern changes in resistance. The testing was conducted at three primary operating voltages of the ACME thruster: 200V, 250V, and 300V. To complement the experimental data, a 0D predictive model was developed to estimate erosion trends, incorporating both erosion rates and circuit properties. This model provided theoretical insights that were crucial for comparing with the actual experimental findings, thereby validating the effectiveness of the new diagnostic method in real-world conditions.

Summary of Results

- Numerical and experimental results show inversely dependent behavior for resistance change over time.
- 0D erosion model was able to predict experimental results with high accuracy.
- Resistance change was able to be resolved over a scale of .05 $\frac{\Omega}{s}$ in the plume with a theoretical resolution of 0.04 $\frac{\Omega}{s}$ at the inner pole.
- Thermal considerations need to be addressed for measurements while in-plume.

The findings from this research highlight the potential of this concept for future applications, particularly in the accelerated lifetime testing of magnetically shielded Hall thrusters. The theoretical resolution at the inner pole is greater than in the plume since the lifetime of the probe is about double for the same overall change in resistance. For future iterations, the focus would be on selecting materials that erode more slowly and are less impacted by external heat sources. Eroding more slowly will able the sensor to be closer to erosion rates of current inner pole materials, like graphite. Copper is a prime example of such a material; it possesses lower thermal conductivity, erodes at a slower rate compared to many other materials, and maintains essential electrical conductivity.

Additionally, a key consideration for future design improvements involves the integration of the circuit in a manner that allows effective measurement of voltage differences. Specifically, this entails devising a method to measure these differences across a strip located on the inner pole of the thruster. Such an integration would be crucial for accurately monitoring and assessing the erosion process, thereby enhancing the reliability and efficiency of lifetime testing for Hall thrusters.

BIBLIOGRAPHY

[1] Vernon H Chaplin, Ryan W Conversano, Alejandro Lopez Ortega, Ioannis G Mikellides, Robert B Lobbia, and Richard R Hofer. Ion velocity measurements in the magnetically shielded miniature (masmi) hall thruster using laser-induced fluorescence. In *36th International Electric Propulsion Conference, University of Vienna, Austria*, 2019.

[2] VH Chaplin, RB Lobbia, A Lopez Ortega, IG Mikellides, RR Hofer, JE Polk, and AJ Friss. Time-resolved ion velocity measurements in a high-power hall thruster using laser-induced fluorescence with transfer function averaging. *Applied Physics Letters*, 116(23), 2020.

[3] Ryan W Conversano, Dan M Goebel, Richard R Hofer, Taylor S Matlock, and Richard E Wirz. Magnetically shielded miniature hall thruster: development and initial testing. In *Proceedings of the thirty-third international electric propulsion conference, Electric Rocket Propulsion Society, Washington DC, USA*, 2013.

[4] Ryan W Conversano, Robert B Lobbia, Steven M Arestie, Alejandro Lopez-Ortega, Vernon H Chaplin, Sean W Reilly, and Dan M Goebel. Demonstration of one hundred kilogram xenon throughput by a low-power hall thruster. *Journal of Propulsion and Power*, 39(2):217–231, 2023.

[5] Ryan W Conversano, Robert B Lobbia, Steven M Arestie, Alejandro Lopez-Ortega, Vernon H Chaplin, Sean W Reilly, and Dan M Goebel. Demonstration of one hundred kilogram xenon throughput by a low-power hall thruster. *Journal of Propulsion and Power*, 39(2):217–231, 2023.

[6] Sarah E Cusson, Benjamin A Jorns, and Alec D Gallimore. Impact of neutral density on the magnetic shielding of hall thrusters. In *36th International Electric Propulsion Conference, University of Vienna, Austria*, 2019.

[7] Ethan T Dale and Benjamin A Jorns. Non-invasive time-resolved measurements of anomalous collision frequency in a hall thruster. *Physics of Plasmas*, 26(1), 2019.

[8] Karl Hoffmann. *Applying the wheatstone bridge circuit*. HBM Darmstadt, Germany, 1974.

[9] Benjamin Jorns, Christopher A Dodson, John R Anderson, Dan M Goebel, Richard R Hofer, Michael J Sekerak, Alejandro Lopez Ortega, and Ioannis G Mikellides. Mechanisms for pole piece erosion in a 6-kw magnetically-shielded hall thruster. In *52nd AIAA/SAE/ASEE Joint Propulsion Conference*, page 4839, 2016.

[10] Hu Li, Kazuhiro Karahashi, Masanaga Fukasawa, Kazunori Nagahata, Tetsuya Tatsumi, and Satoshi Hamaguchi. Sputtering yields and surface chemical modification of tin-doped indium oxide in hydrocarbon-based plasma etching. *Journal of Vacuum Science & Technology A*, 33(6), 2015.

[11] Alejandro Lopez Ortega, Ioannis G Mikellides, Ryan Conversano, Robert B Lobbia, and Vernon H Chaplin. Plasma simulations for the assessment of pole erosion in the magnetically shielded miniature hall thruster (masmi). 2019.

[12] Alejandro Lopez Ortega, Ioannis G Mikellides, Michael J Sekerak, and Benjamin A Jorns. Plasma simulations in 2-d (rz) geometry for the assessment of pole erosion in a magnetically shielded hall thruster. *Journal of Applied Physics*, 125(3), 2019.

[13] David Manzella, Jihn Yim, and Iain Boyd. Predicting hall thruster operational lifetime. In *40th AIAA/ASME/SAE/ASEE Joint Propulsion Conference and Exhibit*, page 3953, 2004.

[14] M Mekhnache, A Drici, L Saad Hamideche, H Benzarouk, A Amara, Linda Cattin, JC Bernede, and M Guerioune. Properties of zno thin films deposited on (glass, ito and zno: Al) substrates. *Superlattices and Microstructures*, 49(5):510–518, 2011.

[15] Ioannis G Mikellides, Ira Katz, Richard R Hofer, and Dan M Goebel. Magnetic shielding of a laboratory hall thruster. i. theory and validation. *Journal of Applied Physics*, 115(4), 2014.

[16] Ioannis G Mikellides and Alejandro Lopez Ortega. Growth of the lower hybrid drift instability in the plume of a magnetically shielded hall thruster. *Journal of Applied Physics*, 129(19), 2021.

[17] Editorial Staff, Sabir Malik., Ps, and NathanW. Rtd wheatstone bridge circuits, Feb 2018.

[18] Peter Thoreau and Justin Little. Influence of field topology on magnetically shielded hall thruster plume divergence. In *2022 IEEE Aerospace Conference (AERO)*, pages 1–8. IEEE, 2022.

[19] Vlad-George Tirila, Alain Demairé, and Charles N Ryan. Review of alternative propellants in hall thrusters. *Acta Astronautica*, 2023.

[20] Thomas Trottenberg, Florian Bansemer, Stephan Böttcher, Davar Feili, Hartmut Henkel, Marcel Hesse, Holger Kersten, Tony Krüger, Jens Laube, Alexey Lazurenko, et al. An in-flight plasma diagnostic package for spacecraft with electric propulsion. *EPJ Techniques and Instrumentation*, 8(1):16, 2021.